

## LONG-TERM INTEGRATION OF THE BAROTROPIC EQUATIONS BY THE LAX-WENDROFF METHOD\*

DAVID HOUGHTON, AKIRA KASAHARA, and WARREN WASHINGTON

National Center for Atmospheric Research, Boulder, Colo.

### ABSTRACT

The system of equations describing the motion of a barotropic fluid with a free surface is solved by using finite-difference methods which are based on the two-step Lax-Wendroff scheme proposed by Richtmyer. The model has rigid boundaries along two latitude circles and the beta-plane approximation is adopted. Initial conditions are given for an ageostrophic jet flow and computations are carried out up to 100 days or 19,200 time steps in order to observe the long-term stability and truncation error properties of the numerical schemes.

A series of integrations is performed using different numerical formulations for the Coriolis term and the boundary conditions. A Fickian type smoothing is introduced to control truncation errors for some of the cases. It is found that the numerical results depend critically upon the method for handling the Coriolis term. One scheme gives a relatively constant total energy during the entire 100 days while the rest of the schemes either develop instability or give damped solutions. All of the solutions differ somewhat after 50 days, thus demonstrating sensitivity to the difference formulation. An additional solution was found for a slightly perturbed initial condition and the solution departed similarly from the other solutions. This suggests that the long-term "deterministic predictability" or sensitivity of the solution of numerical models for large-scale atmospheric motions is as much a function of details in the difference equations as it is of the accuracy in the initial conditions.

### 1. INTRODUCTION

The achievements in short-term numerical weather predictions have encouraged attempts to make long-term numerical predictions. However, there are many obstacles to obtaining meaningful long-term numerical solutions of meteorological equations. For example the effects of numerical stability and truncation error become far more pronounced as short-term integrations are extended to long-term. Similarly, errors or inconsistencies in the initial conditions may have a significant effect on the solution after a large number of time steps.

In this study an attempt is made to derive a satisfactory scheme for the long-term integration of an atmospheric model. By employing a simple barotropic model, many experiments with various finite-difference formulations can be made which enable us to observe sensitivities in the long-term solutions and to examine some of the problems relating to long-term integrations. Many finite-difference schemes have been proposed for integration of the primitive equations. See for example Richtmyer [5] and Shuman [7]. We chose to use formulations based on the two-step Lax-Wendroff scheme proposed by Richtmyer [6], because it has not been tested extensively enough on the atmospheric problems. (See also the original paper by Lax and Wendroff [2].) This Lax-Wendroff scheme was developed to handle equations written entirely in "divergence" form and does not prescribe uniquely the

treatment of boundary conditions or of the Coriolis term. Therefore, in this paper special attention will be given to the handling of the Coriolis term and the boundary conditions. A Fickian type smoothing operator is introduced in some cases to control truncation errors in the numerical solution.

We first study the difference formulations to be sure that the schemes are stable for the linearized equations. This is useful since it sheds light on some of the general tendencies that might be expected in the nonlinear solutions. However, the final test of the methods is in the numerical integrations. Integrations are carried out up to 100 days (19,200 time steps) for a series of nine experiments encompassing various formulations of both the Coriolis term and the boundary conditions. The general behavior of the solutions is examined by observing the computed total energy trend.

The solutions are analyzed further by comparing each with the solution obtained by the "best" scheme. This enables us to observe some of the differences in the solutions due to the nature of the stability and the truncation error of the schemes. In order to exhibit the sensitivity of this barotropic model, an integration is performed with the "best" difference scheme and initial conditions having a slight "error."

### 2. PHYSICAL MODEL

The model used in this study is an incompressible, homogeneous, inviscid, and hydrostatic fluid confined in a channel corresponding to a middle-latitude band on the

\*A portion of this paper was presented at the 237th National Meeting of the American Meteorological Society, April 1965, Washington, D.C., under the title "Predictability in a Numerical Prediction Model."

earth. The lower surface is flat and rigid, but the upper surface is free. The northern and southern boundaries, 4,800 km. apart, are rigid "walls," where the north-south component of velocity vanishes. The flow is assumed to be periodic in the east-west direction with a wavelength of 5,760 km. The beta-plane approximation is used.

In order to reduce the speed of gravity waves in this one-layer model, an inert fluid of infinite depth is placed above the fluid of interest. The pressure gradients in the lower fluid depend only upon the slope of the interface between the fluids multiplied by a value proportional to the difference in the densities of the two fluids. Therefore, the model is equivalent to a one-layer model with a reduced acceleration of gravity. The value of reduced acceleration of gravity is taken as 1.4 m. sec.<sup>-2</sup> which means the density of the upper layer is 0.86 of that in the lower layer.

The basic equations for this model in Eulerian form are

$$\frac{\partial u}{\partial t} + u \frac{\partial u}{\partial x} + v \frac{\partial u}{\partial y} - fv + g \frac{\partial h}{\partial x} = 0, \quad (2.1)$$

$$\frac{\partial v}{\partial t} + u \frac{\partial v}{\partial x} + v \frac{\partial v}{\partial y} + fu + g \frac{\partial h}{\partial y} = 0, \quad (2.2)$$

$$\frac{\partial h}{\partial t} + u \frac{\partial h}{\partial x} + v \frac{\partial h}{\partial y} + h \left( \frac{\partial u}{\partial x} + \frac{\partial v}{\partial y} \right) = 0. \quad (2.3)$$

Variables are defined as follows:

- $x, y$ : east-west and north-south coordinates
- $u, v$ : velocity components in the  $x$ - and  $y$ -directions
- $t$ : time
- $h$ : depth of the fluid
- $f$ : Coriolis parameter
- $g$ : reduced acceleration of gravity.

The equation for total energy (potential plus kinetic) integrated over the channel derived from (2.1)–(2.3) is

$$\frac{\partial E}{\partial t} = -D_p \quad (2.4)$$

where  $E$  is the total energy defined by

$$E = \iint_{\sigma} \frac{1}{2} (u^2 + v^2 + gh) h d\sigma. \quad (2.5)$$

Here  $\sigma$  is the total area of integration and  $D_p$  is the rate of energy dissipation which vanishes for an inviscid fluid. Thus, the total energy is conserved in this model.

### 3. DIFFERENCE EQUATIONS

For a given set of differential equations, it is always possible to write down various forms of difference equations corresponding to the given set. It is one of the objects in this study to compare the solutions of various difference equations, which are all formulated based on the two-step Lax-Wendroff scheme proposed by Richtmyer [6].

Let us rewrite (2.1) to (2.3) in the following "divergence" form and add a Fickian type smoothing term for the purpose of controlling truncation errors:

$$\frac{\partial U}{\partial t} + \frac{\partial P}{\partial x} + \frac{\partial Q}{\partial y} = fR + \nu h_0^{-1} h \nabla^2 M \quad (3.1)$$

where  $U, P, Q, R,$  and  $M$  are the column matrices defined by

$$U = \begin{pmatrix} m \\ n \\ h \end{pmatrix}, \quad P = \begin{pmatrix} \frac{m^2}{h} + \frac{1}{2} gh^2 \\ \frac{mn}{h} \\ m \end{pmatrix}, \quad Q = \begin{pmatrix} \frac{mn}{h} \\ \frac{n^2}{h} + \frac{1}{2} gh^2 \\ n \end{pmatrix},$$

$$R = \begin{pmatrix} n \\ m \\ 0 \end{pmatrix}, \quad \text{and} \quad M = \begin{pmatrix} m \\ n \\ 0 \end{pmatrix}$$

in which  $m = hu$  and  $n = hv$ . Also in (3.1),

$$\nabla^2 = \frac{\partial^2}{\partial x^2} + \frac{\partial^2}{\partial y^2}$$

$h_0$  is a mean depth of the fluid and  $\nu$  is the coefficient of smoothing. Note that the Fickian type smoothing represents viscous dissipation in the fluid. Upon applying the boundary conditions of the problem, the rate of energy dissipation  $D_p$  now takes the form,

$$D_p = \nu h_0^{-1} \iint_{\sigma} [(\nabla(hu))^2 + (\nabla(hv))^2] d\sigma$$

which is non-negative and decreases the total energy of the numerical solution with time.

Let us denote any function  $S(x, y, t)$  of  $x = j\Delta x, y = k\Delta y,$  and  $t = l\Delta t$  as  $S_{j,k}^l$  where  $j, k,$  and  $l$  are integers. In this problem, the space increment  $\Delta x$  is taken equal to  $\Delta y$  both of which are denoted by  $\Delta s$ . The time increment is denoted by  $\Delta t$ . The two-step difference equations used for (3.1) consist of the following two equations which are used at alternate time cycles.

$$\left. \begin{aligned} U_{j,k}^{l+1} &= \bar{U}_{j,k} - \frac{1}{2}\sigma[\Delta_x P_{j,k}^l + \Delta_y Q_{j,k}^l] \\ &- F\{\alpha R_{j,k}^l + (1-\alpha)[(1-\epsilon)\bar{R}_{j,k}^l + \epsilon R_{j,k}^{l+1}]\} \\ &+ KH_{j,k}^{l-1} \nabla^2 M_{j,k}^{l-1} \end{aligned} \right\}, \quad (3.3a)$$

$$\left. \begin{aligned} U_{j,k}^{l+2} &= U_{j,k}^l - \sigma[\Delta_x P_{j,k}^{l+1} + \Delta_y Q_{j,k}^{l+1}] \\ &- 2F\{\alpha R_{j,k}^{l+1} + (1-\alpha)[(1-\epsilon)R_{j,k}^l + \epsilon R_{j,k}^{l+2}]\} \\ &+ 2KH_{j,k}^l \nabla^2 M_{j,k}^l \end{aligned} \right\}, \quad (3.3b)$$

where

$$\bar{U}_{j,k} = \frac{1}{4}(U_{j+1,k}^l + U_{j-1,k}^l + U_{j,k+1}^l + U_{j,k-1}^l), \quad (3.4)$$

$$\nabla^2 M_{j,k}^i = 4(\bar{M}_{j,k}^i - M_{j,k}^i), \quad (3.5)$$

$$\Delta_x P_{j,k}^i = P_{j+1,k}^i - P_{j-1,k}^i, \quad (3.6)$$

$$\Delta_y Q_{j,k}^i = Q_{j,k+1}^i - Q_{j,k-1}^i, \quad (3.7)$$

$$\sigma = \Delta t / \Delta s, \Delta s = \Delta x = \Delta y, K = \nu \frac{\Delta t}{(\Delta s)^2},$$

$$F = f \Delta t, H_{j,k}^i = h_{j,k}^i h_0^{-1}.$$

The averaging operator defined by (3.4) applies also for  $R_{j,k}^i$  and  $M_{j,k}^i$ .

Note that (3.3a,b) are applied only in the interior of the integration domain. The special treatments along the boundaries will be discussed later. In (3.3a, b), the symbols  $\alpha$  and  $\epsilon$  are parameters, which determine different formulations of the Coriolis term. As noted in the introduction, the Lax-Wendroff system does not prescribe the formulation for the Coriolis term, so we are at liberty to try many formulations. The Coriolis term is important to attain the geostrophic balance, and it might be expected that the various formulations of the Coriolis term would cause appreciable differences in the solutions. We shall consider the following four different formulations.

**SCHEME A,  $\alpha=1$**

The expression for the Coriolis term, which we shall denote by *CL* henceforth, is

$$CL = -FR_{j,k}^i \text{ in (3.3a)}$$

and

$$CL = -2FR_{j,k}^{i+1} \text{ in (3.3b).}$$

Thus, the Coriolis term is evaluated explicitly at the time level,  $l$ , in the first step and in the second step, it is evaluated at the time level,  $l+1$ , which is midway between  $l$  and  $l+2$ . We shall refer to Scheme A as the "explicit and midway" formulation.

**SCHEME B,  $\alpha=0$  and various values of  $\epsilon$ .**

In this case, we have

$$CL = -F[(1-\epsilon)\bar{R}_{j,k}^i + \epsilon R_{j,k}^{i+1}] \text{ in (3.3a)}$$

and

$$CL = -2F[(1-\epsilon)R_{j,k}^i + \epsilon R_{j,k}^{i+2}] \text{ in (3.3b).}$$

The parameter  $\epsilon(0 \leq \epsilon \leq 1)$  determines a weighted average of the Coriolis terms between different time levels. The following three different values of  $\epsilon$  are considered:

**SCHEME B1:  $\alpha=0, \epsilon=0$ .**

The Coriolis term is evaluated at a time level lagged  $\Delta t/2$  in step 1 and lagged  $\Delta t$  in step 2 respectively. We shall refer to this as the "explicit-lagging" formulation.

**SCHEME B2:  $\alpha=0, \epsilon=0.5$ .**

The Coriolis term is evaluated as the arithmetic average of the two Coriolis terms at two consecutive levels. We shall refer to this case as the "averaging" formulation.

**SCHEME B3:  $\alpha=0, \epsilon=1.0$ .**

The Coriolis term is evaluated at the time level advanced  $\Delta t/2$  in step 1 and advanced  $\Delta t$  in step 2, respectively. We shall refer to this case as the "implicit" formulation.

Let us now discuss the boundary conditions. The periodic boundary conditions at the eastern and western boundaries are easily handled by adding one extra column of grid points outside the eastern and western boundaries respectively. Because of the periodicity conditions, the values of dependent variables at the additional grid points are obtained directly from the grid points of the column next to the boundary at the opposite side of the integration domain.

Special handling is required at the northern and southern boundaries. There, the  $y$  component of the velocity,  $v$ , vanishes at all times but the  $x$  component of the velocity,  $u$ , and the height,  $h$ , must be computed from (3.3a, b). We require one additional assumption to evaluate the Laplacian operator  $\nabla^2$  and the averaging operator  $\bar{U}_{j,k}^i$  defined by (3.5) and (3.4). We assume that the derivative  $\partial U / \partial y$  vanishes at these boundaries which means that the operators are evaluated by taking that  $U_{j,k+1}^i = U_{j,k-1}^i$  in (3.4), which corresponds to the free slip condition for viscous flow.

There is no problem in the evaluation of  $\Delta_x P$  defined by (3.6) on the northern and southern boundaries. The problem is how to evaluate  $\Delta_y Q$  there. Since the advection operators defined by (3.6) and (3.7) have second-order accuracy, it is desirable to evaluate  $\Delta_y Q$  with second-order accuracy at the boundaries. A usual practice in this respect, however, is to use the first-order uncentered difference for this evaluation. Therefore, in this study we shall run calculations using both the first- and second-order non-centered differences for  $\Delta_y Q$  at the boundaries and compare the two results. Thus, the  $\Delta_y Q$  defined by (3.7) is expressed as

$$\Delta_y Q_{j,N}^i = 2\gamma(Q_{j,N}^i - Q_{j,N-1}^i) + (1-\gamma)(3Q_{j,N}^i - 4Q_{j,N-1}^i + Q_{j,N-2}^i) \quad (3.8a)$$

where the index  $N$  represents the grid points on the northern boundary and

$$\Delta_y Q_{j,O}^i = 2\gamma(Q_{j,1}^i - Q_{j,O}^i) - (1-\gamma)(Q_{j,2}^i - 4Q_{j,1}^i + 3Q_{j,O}^i) \quad (3.8b)$$

where the index  $O$  represents the grid points on the southern boundary. The parameter  $\gamma$  takes either 1 or 0 depending on whether the difference operator has first-order or second-order accuracy.

**4. STABILITY ANALYSIS**

In order to illuminate differences in the properties of the difference schemes described in the previous section, we shall discuss the stability conditions of these schemes. The study of computational stability for difference equations becomes more important when one attempts to

integrate the equations for a long term. In this study, we shall be concerned only with the stability of difference schemes in the von Neumann sense, namely the stability of the corresponding linearized system with constant coefficients. Moreover, for simplicity, we will deal with only the one-dimensional system.

If we introduce new dimensionless variables

$$u' = u(g\bar{H})^{-1/2}, v' = v(g\bar{H})^{-1/2}, \text{ and } h' = hH^{-1} \quad (4.1)$$

where  $\bar{H}$  is an averaged height (constant) of the free surface, the one-dimensional linearized version of the system of (2.1)–(2.3) may be written as

$$\frac{\partial u'}{\partial t} + \bar{U} \frac{\partial u'}{\partial x} + \bar{C} \frac{\partial h'}{\partial x} - fv' - \nu \frac{\partial^2 u'}{\partial x^2} = 0, \quad (4.2)$$

$$\frac{\partial v'}{\partial t} + \bar{U} \frac{\partial v'}{\partial x} + fu' - \nu \frac{\partial^2 v'}{\partial x^2} = 0, \quad (4.3)$$

$$\frac{\partial h'}{\partial t} + \bar{U} \frac{\partial h'}{\partial x} + \bar{C} \frac{\partial u'}{\partial x} = 0. \quad (4.4)$$

in which  $\bar{U}$  denotes an averaged zonal velocity (constant) and  $\bar{C} = (g\bar{H})^{1/2}$ . For simplicity, we shall omit writing primes in further references to (4.2)–(4.4).

The next step is to write difference equations for (4.2)–(4.4) corresponding to the formulas (3.3a, b). To save space, we shall omit writing the equations. Into the resulting equations, we substitute the following Fourier terms  $u_j^i \exp(i\kappa j\Delta x)$  for  $u_j^i$ , and similar expressions for  $v_j^i$  and  $h_j^i$  to eliminate the space dependence of the dependent variables. The symbol  $\kappa$  denotes the wave number. The resulting equations are as follows:

$$u^{i+1} = Ev^{i+1} + Au^i + Bv^i - Gh^i + Du^{i-1}, \quad (4.5)$$

$$v^{i+1} = -Eu^{i+1} - Bu^i + Av^i + Dv^{i-1}, \quad (4.6)$$

$$h^{i+1} = -Gu^i + Ah^i, \quad (4.7)$$

$$u^{i+2} = Sv^{i+2} - 2Nu^{i+1} + Tv^{i+1} - 2Gh^{i+1} + Mu^i + Wv^i, \quad (4.8)$$

$$v^{i+2} = -Su^{i+2} - Tu^{i+1} - 2Nv^{i+1} - Wu^i + Mv^i, \quad (4.9)$$

$$h^{i+2} = -2Gu^{i+1} - 2Nh^{i+1} + h^i \quad (4.10)$$

where

$$\begin{aligned} A &= \cos \mu - iU \sin \mu & K &= \nu \Delta t / (\Delta x)^2 \\ B &= F(1-\epsilon)(1-\alpha) \cos \mu & M &= 1 + 2D \\ &+ F\alpha & N &= iU \sin \mu \\ C &= \bar{C} \Delta t / \Delta x & S &= 2F\epsilon(1-\alpha) \\ D &= 2K(\cos \mu - 1) & T &= 2F\alpha \\ E &= \epsilon F(1-\alpha) & U &= \bar{U} \Delta t / \Delta x \\ F &= f \Delta t & W &= 2F(1-\epsilon)(1-\alpha) \\ G &= iC \sin \mu & & \\ & & & \mu = \kappa \Delta x. \end{aligned} \quad (4.11)$$

The right-hand sides of (4.5)–(4.10) contain quantities which have the same time index as appears on the left hand sides. Therefore, in order to arrange matters so that the right hand sides contain only quantities which have time indices lower than the ones appearing on the left hand sides, we have to make some eliminations of appropriate variables. The result of such eliminations is

$$\begin{pmatrix} u^{i+1} \\ v^{i+1} \\ h^{i+1} \\ u^{i+2} \\ v^{i+2} \\ h^{i+2} \end{pmatrix} = a \begin{pmatrix} u^{i-1} \\ v^{i-1} \\ h^{i-1} \\ u^i \\ v^i \\ h^i \end{pmatrix} \quad (4.12)$$

where  $a$  is the amplification matrix which is the function of the physical parameters  $U, C, F, K$ , and  $\mu$ . The expressions for the elements of the matrix,  $a_{j,k}$ , are lengthy and to save space we omit writing them here. The eigenvalues of the matrix  $a$  are the roots  $\{\lambda\}$  of the characteristic equation

$$|a - \lambda I| = 0 \quad (4.13)$$

where  $I$  is the unit matrix. Since the system under consideration is a physically stable system, the stability condition requires that the eigenvalues do not exceed unity in absolute value. The evaluation of the eigenvalues of the square matrix of order 6 can be made numerically for various values of the parameters  $U, C, F, K$ , and  $\mu$ . However, in order to understand the roles played by these parameters in the stability condition, it is best to discuss simpler situations first.

CASE (1)  $F=K=0, U \neq 0, C \neq 0$ .

In this case, we omit terms involving the Coriolis parameter and smoothing. The amplification matrix  $a$  reduces to a square matrix of order 3 and the three eigenvalues are easily found

$$\lambda = 1 - w^2(1 - \cos 2\mu) - iw \sin 2\mu \quad (4.14)$$

where  $w$  stands for the three different values,  $U \pm C$  and  $U$ . The magnitude of  $\lambda$  is given by

$$\begin{aligned} |\lambda|^2 &= [1 - w^2(1 - \cos 2\mu)]^2 + w^2 \sin^2 2\mu \\ &= 1 - w^2(1 - w^2)(1 - \cos 2\mu)^2. \end{aligned}$$

The largest possible value of  $w$  is  $|U| + C$ ; hence  $|\lambda|^2 \leq 1$  if

$$\frac{\Delta t}{\Delta x} [|\bar{U}| + (g\bar{H})^{1/2}] \leq 1. \quad (4.15)$$

It should be pointed out that the magnitude of the eigenvalues becomes unity at  $\mu=0$  and  $\mu=\pi$ ; and the minima appear at  $\mu=\pi/2$  and  $\mu=3\pi/2$  under the condition (4.15). Since  $\mu = \kappa \Delta x$  and  $\kappa$  is the wave number defined by  $\kappa = 2\pi/L$  where  $L$  is the wavelength, the case

of  $\mu=\pi$  corresponds to that of  $L=2\Delta x$  and  $|\lambda|=1$ ; and the case of  $\mu=\pi/2$  corresponds to  $L=4\Delta x$  and  $|\lambda|$  is minimum. This implies that the  $2\Delta x$ -wave component will not be damped, although the  $4\Delta x$ -wave component will be damped effectively. Therefore, if a long-term integration is made using the two-step Lax-Wendroff scheme, it is very probable that the  $2\Delta x$ -wave component will eventually dominate.

CASE (2)  $U=C=K=0, F\neq 0$ .

In this case (4.2)-(4.4) reduce to

$$\frac{\partial u}{\partial t} - fv = 0, \frac{\partial v}{\partial t} + fu = 0. \tag{4.16}$$

This system describes inertia motions and it can be written in the form

$$\frac{\partial Z}{\partial t} + i f Z = 0 \tag{4.17}$$

with  $Z$  defined by

$$Z = u + iv, i = (-1)^{1/2}.$$

The difference equations analogous to (3.3a, b) in this case may be written as

$$Z_j^{i+1} = \bar{Z}_j - iF\{\alpha Z_j + (1-\alpha)[(1-\epsilon)\bar{Z}_j + \epsilon Z_j^{i+1}]\}, \tag{4.18a}$$

$$Z_j^{i+2} = Z_j - 2iF\{\alpha Z_j^{i+1} + (1-\alpha)[(1-\epsilon)Z_j + \epsilon Z_j^{i+2}]\} \tag{4.18b}$$

where  $F=f\Delta t$ . After substituting the Fourier terms  $Z^i \exp(i\kappa j\Delta x)$  into (4.18a, b) and eliminating  $Z^{i+1}$  between the resulting equations, we obtain

$$Z^{i+2} = \Omega Z^i$$

where

$$\Omega = \frac{1-2iF(1-\alpha)(1-\epsilon)}{1+2iF(1-\alpha)\epsilon} - \frac{2i\alpha F[\cos \mu - iF(1-\alpha)(1-\epsilon) \cos \mu - iF\alpha]}{[1+iF\epsilon(1-\alpha)][1+2iF(1-\alpha)\epsilon]}, \tag{4.19}$$

which is the amplification factor. We shall evaluate the magnitude of  $\Omega$  for the following cases.

**SCHEME A.**  $\alpha=1$  ("explicit and midway" formulation).

In this case, (4.19) reduces to

$$\Omega = 1 - 2iF(\cos \mu - iF)$$

and

$$|\Omega|^2 = (1-2F^2)^2 + 4F^2 \cos^2 \mu.$$

The maxima of  $|\Omega|^2$  occur at  $\mu=0$  and  $\mu=\pi$  and

$$|\Omega|_{\max}^2 = 1 + 4F^4 = 1 + 4(f\Delta t)^4.$$

It is seen that the magnitude of  $\Omega$  is larger than unity. The values of amplification  $[1+4(f\Delta t)^4]^{N/2}$  at various cycles  $N$  for  $\Delta t=7.5$  min. are shown in the second column in table 1. A similar scheme has been investigated by Williamson [8].

**SCHEME B1.**  $\alpha=0, \epsilon=0$  ("explicit-lagging" formulation). In this case, (4.19) reduces to

$$\Omega = 1 - 2iF$$

and

$$|\Omega|^2 = 1 + 4F^2 = 1 + 4(f\Delta t)^2.$$

The values of amplification  $[1+4(f\Delta t)^2]^{N/2}$  at various cycles  $N$  for  $\Delta t=7.5$  min. are shown in the third column in table 1. Note that Scheme B1 yields a large amplification and is not suitable for a long-term integration.

**SCHEME B2.**  $\alpha=0, \epsilon=0.5$  ("averaging" formulation).

In this case, (4.19) reduces to

$$\Omega = \frac{1-iF}{1+iF}$$

and

$$|\Omega|^2 = 1.$$

This scheme, therefore, is neutral.

**SCHEME B3.**  $\alpha=0, \epsilon=1.0$  ("implicit" formulation).

In this case, (4.19) reduces to

$$\Omega = \frac{1}{(1+2iF)}$$

and

$$|\Omega|^2 = (1+4F^2)^{-1}.$$

The values of amplification  $[1+4(f\Delta t)^2]^{-N/2}$  at various cycles  $N$  and  $\Delta t=7.5$  min. are shown in the fourth column in table 1. Note that Scheme B3 causes damping of the solution.

**CASE (3)**  $U=C=F=0, K\neq 0$ .

In this case, it is sufficient to consider only (4.2) which reduces to

$$\frac{\partial u}{\partial t} = \nu \frac{\partial^2 u}{\partial x^2}. \tag{4.20}$$

The two-step difference formulation of (4.20) may be written as

$$u_j^{i+1} = \bar{u}_j + K(u_{j+1}^{i-1} - 2u_j^{i-1} + u_{j-1}^{i-1}), \tag{4.21a}$$

$$u_j^{i+2} = u_j^i + K(u_{j+1}^i - 2u_j^i + u_{j-1}^i) \tag{4.21b}$$

where  $K = \nu\Delta t / (\Delta x)^2$ .

After substituting the Fourier terms  $u^i \exp(i\kappa j\Delta x)$  into (4.21), the resulting equations in the following matrix form are derived:

$$\begin{pmatrix} u^{i+1} \\ u^{i+2} \end{pmatrix} = b \begin{pmatrix} u^{i-1} \\ u^i \end{pmatrix}$$

TABLE 1.—The values of amplification for  $f=10^{-4}$  sec.<sup>-1</sup> and  $\Delta t=7.5$  min.

$N$	$[1+4(f\Delta t)^4]^{N/2}$	$[1+4(f\Delta t)^2]^{N/2}$	$[1+4(f\Delta t)^2]^{-N/2}$
1	1.000082	1.00404	0.995974
10	1.0000820	1.04116	0.960466
10 <sup>2</sup>	1.0008205	1.49686	0.668066
10 <sup>3</sup>	1.0082349	56.47	0.177089×10 <sup>-1</sup>
10 <sup>4</sup>	1.0854688	3.30×10 <sup>17</sup>	3.033×10 <sup>-18</sup>

where

$$b = \begin{pmatrix} 2K(\cos \mu - 1) & \cos \mu \\ 0 & 1 + 4K(\cos \mu - 1) \end{pmatrix}.$$

The eigenvalues of  $b$  are readily found; they are

$$\lambda_1 = 2K(\cos \mu - 1), \lambda_2 = 1 + 4K(\cos \mu - 1).$$

The stability requirement that the eigenvalues should not exceed unity in magnitude establishes the stability condition that

$$K \leq \frac{1}{4} \text{ or } \frac{\nu \Delta t}{(\Delta x)^2} \leq \frac{1}{4}$$

Note that the magnitude of  $\lambda_{1,2}$  is less than unity for  $\mu \neq 0$  and  $K < \frac{1}{4}$ .

CASE (4)  $F=0, U \neq 0, C \neq 0, K \neq 0$ .

In this case, the amplification matrix  $a$  in (4.12) is a square matrix of order 6. The eigenvalues of  $a$  are evaluated numerically by using a subroutine, EIG 4, written by B. N. Parlett. Figure 1 illustrates the domain of stability shown using the  $(|U|, C)$  coordinate plane for various values of  $K$ .

CASE (5)  $U \neq 0, C \neq 0, K \neq 0, F \neq 0$ .

This is the general case. Equation (4.13) was solved numerically to obtain the eigenvalues. To save computing time, the value of  $F$  was taken to be 0.045 corresponding to  $\Delta t = 7.5$  min. and the value of  $K$  was taken to be 0.00273 corresponding to  $\nu = 3.5 \times 10^5 \text{ m}^2 \text{ sec}^{-1}$ . These values of  $F$  and  $K$  appear to be so small that the stability criterion for this general case may be expressed in practice by combining the stability conditions discussed separately in Cases (1), (2), and (3).

### 5. INITIAL CONDITIONS

Identical initial conditions are used in all of the numerical experiments except for the one case in which the growth of a small initial "error" is investigated. The initial conditions represent a westerly jet flow with a small north-south undulation along the jet axis. In order to suppress unwanted gravity-inertial waves from the solution, the initial height and velocity fields are prescribed from a given stream function field as follows:

The initial height field is obtained from the prescribed stream function field by requiring the following balance condition to be satisfied:

$$\nabla^2 h = \frac{f}{g} \nabla^2 \psi - \frac{2}{g} \left[ \left( \frac{\partial^2 \psi}{\partial x \partial y} \right)^2 - \frac{\partial^2 \psi}{\partial y^2} \frac{\partial^2 \psi}{\partial x^2} \right] + \frac{\beta}{g} \frac{\partial \psi}{\partial y} \quad (5.1)$$

where  $\beta = \partial f / \partial y$ . The terms on the right hand side of (5.1) are evaluated in the interior of the channel. In order to solve the Poisson equation (5.1) for  $h$ , the values on the boundaries must be specified. The values on the eastern and western boundaries are easily obtained from the periodicity conditions. The values on the northern and southern boundaries are two different constants  $\bar{h}_N$  and  $\bar{h}_S$  which are calculated from

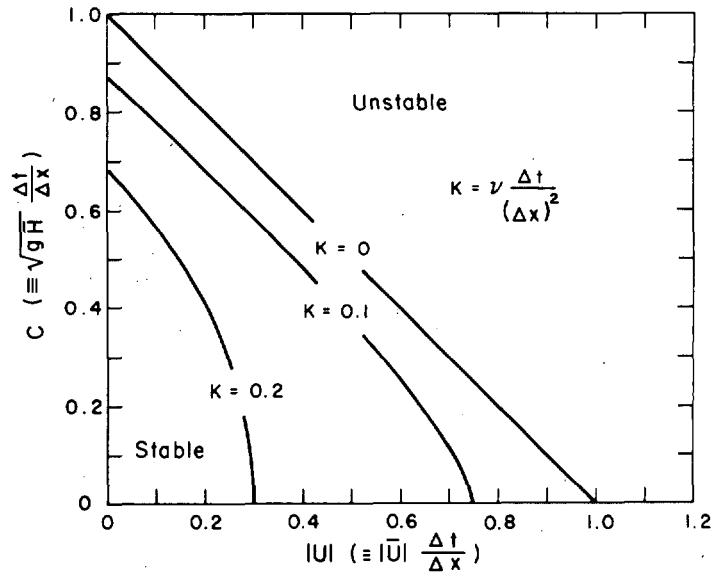


FIGURE 1.—The domain of stability shown on the  $(|U|, C)$  coordinate plane for various values of  $K$ .

$$\bar{h}_N = h_0 + \frac{1}{g} \int_0^{W/2} f \frac{\partial \bar{\psi}}{\partial y} dy \quad (5.2)$$

where  $\bar{\psi} = \frac{1}{L} \int_0^L \psi dx$ , and  $y=0$  is located in the middle of the channel where  $\bar{h} = h_0$ . Here  $W$  is the width of the channel and  $L$  is the basic wavelength in the east-west direction. Likewise,  $\bar{h}_S$  is obtained from (5.2) except that the upper integration limit is replaced by  $-W/2$ .

The divergent part of the velocity field is computed from the prescribed stream function field with a quasi-geostrophic divergence equation suggested by Phillips [3]:

$$\frac{gh_0}{\bar{f}} \nabla^2 D - \bar{f} D + \left( \frac{\partial}{\partial x} \nabla^2 \psi \right) \frac{\partial \psi}{\partial y} - \left( \frac{\partial}{\partial y} \nabla^2 \psi \right) \frac{\partial \psi}{\partial x} - \beta \frac{\partial \psi}{\partial x} = 0 \quad (5.3)$$

where  $D$  is the divergence and  $\bar{f}$  an average value of the Coriolis parameter. In order to solve (5.3), the assumption is made that the divergence vanishes on the northern and southern boundaries. The periodicity conditions are applied at the eastern and western boundaries.

The velocity potential,  $\chi$ , is then obtained from the divergence by the relationship,

$$\nabla^2 \chi = D, \quad (5.4)$$

assuming the velocity potential to be zero at both the northern and southern boundaries.

Finally the velocity components are obtained from the stream function and velocity potential by the relationships,

$$u = -\frac{\partial \psi}{\partial y} + \frac{\partial \chi}{\partial x} \text{ and } v = \frac{\partial \psi}{\partial x} + \frac{\partial \chi}{\partial y} \quad (5.5)$$

The initial stream function is given by

$$\psi(x, y) = -\psi_0 \tan^{-1} \left[ \frac{y - y_0 - q \sin \frac{2\pi x}{L}}{d} \right] \quad (5.6)$$

where  $\psi$  is the stream function,  $\psi_0$  is the amplitude,  $y_0$  is the mean latitude of the jet axis,  $q$  is the north-south amplitude of the jet axis, and  $d$  is a parameter which determines the width of the jet. Since the stream function should be constant along each of the northern and southern boundaries to be consistent with the condition that  $v=0$  there, (5.6) cannot be used right up to these boundaries. Instead (5.6) is applied to within three grid positions from each boundary and then a linear  $y$ -direction gradient is assumed between there and the boundary. The boundary value is set equal to the zonal average of the stream function three grid distances away as prescribed by (5.6) for each boundary respectively.

In the numerical calculations the following values are adopted:

$$\begin{aligned} \psi_0 &= 1.44 \times 10^7 \text{ m.}^2 \text{ sec.}^{-1} & g &= 1.4 \text{ m. sec.}^{-2} \\ y_0 &= 11\Delta s & \bar{f} &= 10^{-4} \text{ sec.}^{-1} \\ q &= \Delta s & \beta &= 1.57 \times 10^{-11} \text{ sec.}^{-1} \text{ m.}^{-1} \\ L &= 24\Delta s & & \text{(value at the latitude} \\ d &= 2\Delta s & & \text{43}^\circ \text{ N.)} \\ h_0 &= 5000 \text{ m.} & \Delta s &= 240,000 \text{ m.} \end{aligned}$$

The time increment,  $\Delta t$ , is set equal to 450 sec. to satisfy the stability requirements discussed in the previous section. The basic grid is 24 x 21 in the east-west and north-south directions respectively.

Figure 2 shows the initial height field used for the experiments. In the experiment where a small initial error is introduced, the height at the center grid point is increased by 0.1 percent. This change is too small to be noticed in the height field as presented in figure 2.

### 6. RESULTS

Nine experiments were made. Eight of these used different values of  $\alpha$ ,  $\epsilon$ , and  $\gamma$  in the finite-difference equations (3.3a, b) and (3.8a, b) together with various values for the coefficient of Fickian smoothing henceforth referred to as the coefficient of smoothing. A tabulation of these experiments is given in table 2. The last experi-

TABLE 2.—Experiments performed

Experiment	Coriolis term	Coefficient of Smoothing (m. <sup>2</sup> sec. <sup>-1</sup> )	Boundary Condition
A.....	Explicit and mid-way ( $\alpha=1$ ).....	$3.5 \times 10^8$	First Order
B.....	Explicit and mid-way ( $\alpha=1$ ).....	0	First Order
C.....	Explicit and mid-way ( $\alpha=1$ ).....	$3.5 \times 10^8$	First Order
D.....	Explicit and mid-way ( $\alpha=1$ ).....	$3.5 \times 10^8$	Second Order.
E.....	Explicit and mid-way ( $\alpha=1$ ).....	0	Second Order.
F.....	Explicit lagging ( $\alpha=0, \epsilon=0$ ).....	0	First Order
G.....	Averaging ( $\alpha=0, \epsilon=0.5$ ).....	0	First Order
H.....	Implicit ( $\alpha=0, \epsilon=1.0$ ).....	0	First Order
I.....	Explicit and mid-way ( $\alpha=1$ ).....	$3.5 \times 10^8$	First Order

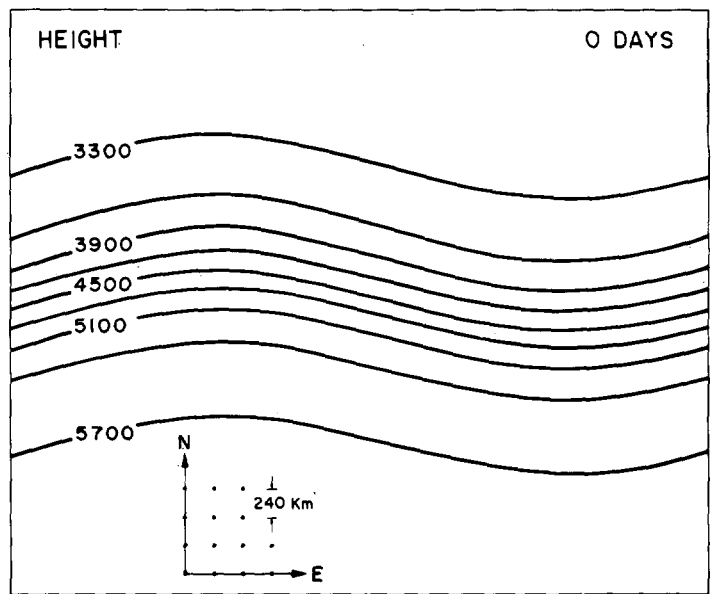


FIGURE 2.—Initial height field in meters as used for the calculations. The 0.1 percent error in the height in one of the experiments is too small to be represented. The grid spacing is shown to the scale of the map in the lower left corner.

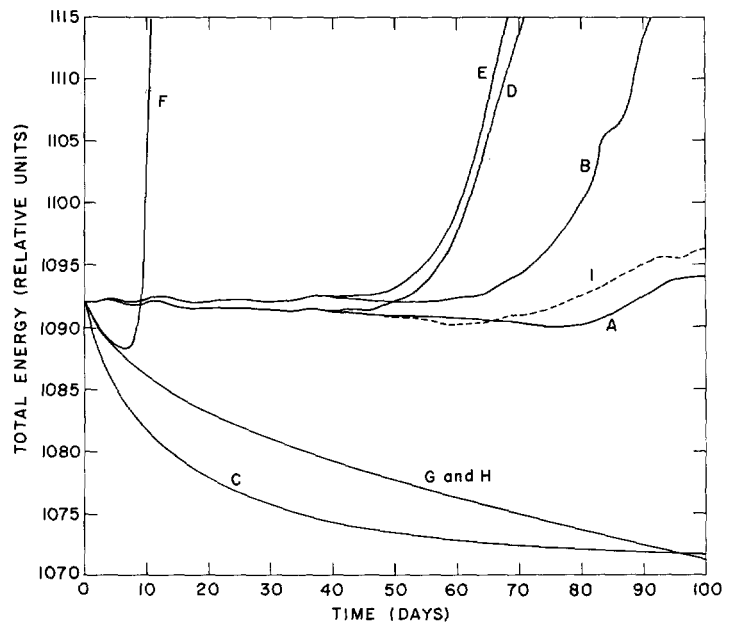


FIGURE 3.—Total energy of the model plotted against time for each of the nine experiments.

ment I is identical to the first one, A, except for a small difference in the initial conditions. The large value for the coefficient of smoothing in experiment C corresponds to the value of kinematic eddy viscosity derived by Richardson [4] to simulate the effect of motions at scales too small to be explicitly represented in the grid.

Figure 3 shows the computed total energy defined by (2.5) for each of the nine experiments. The effect of the Coriolis formulation on the solution is clearly evident. Experiments B, F, G, and H demonstrate the differences,

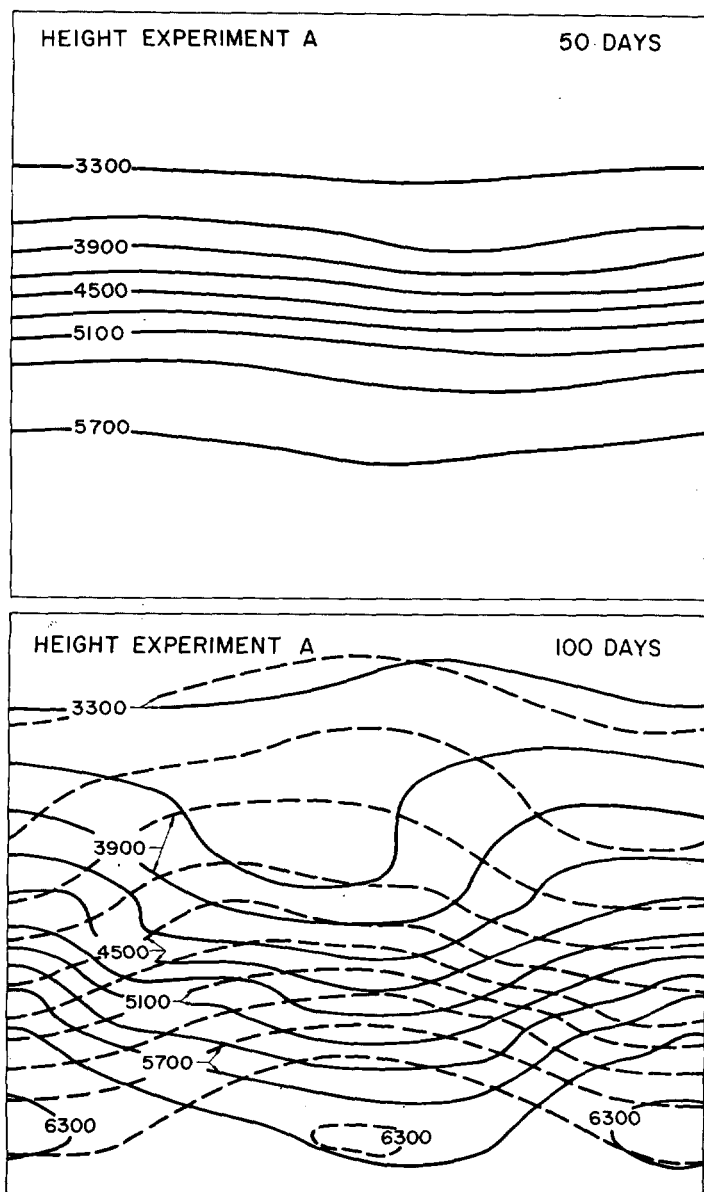


FIGURE 4.—(a) Height field for experiment A after 50 days. (b) Height field for experiment A after 100 days. The solutions given by the two partial sets of the grid network are shown separately, with solid and dashed lines. See text.

for they are similar in all respects except for the Coriolis formulation. As predicted by the stability analysis, experiment F shows an instability and experiment H shows a damped solution. The very nearly neutral stability for the "Explicit and mid-way" Coriolis formulation is consistent with the relatively constant energy in experiment B for the first 60 days. The damping in experiment G and its similarity to experiment H may not be explained by linear stability considerations only.

Experiments A, B, C, D, E, and I all have the same Coriolis formulation, the one which appears to give the most neutral results. From these results it may be concluded that the second-order boundary conditions

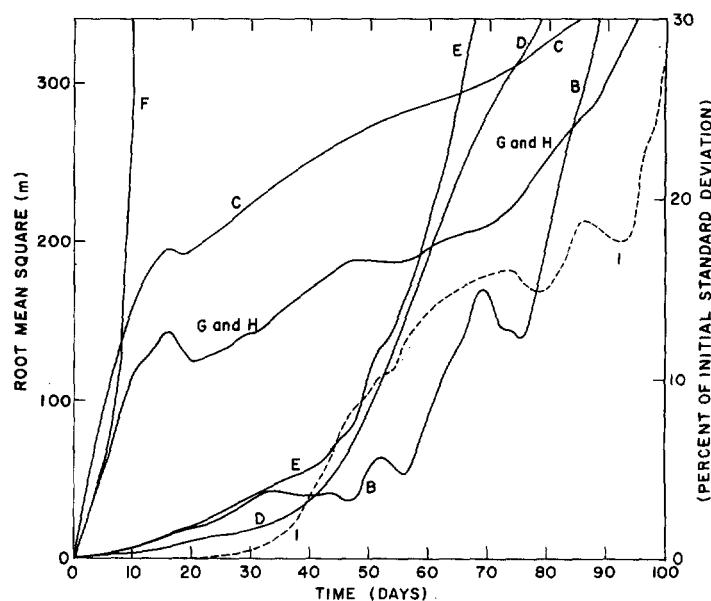


FIGURE 5.—Root mean square of the difference in height field between experiment A and each of the other experiments averaged over the entire domain. The scale on the right expresses the root mean square value in units of the standard deviation in the height field in the initial conditions, the quantity being identical for all the experiments except experiment I which differs ever so slightly.

tend to be more unstable compared with the first-order boundary conditions (comparing A and B to D and E respectively). In addition it may be observed that the Fickian smoothing tends to stabilize the solutions (comparing A and D to B and E, respectively) although a larger smoothing, as introduced in C, has a large damping effect.

The development of instability in experiments B, D, and E after a long time period may be considered due to both the Coriolis formulation and the separation of two loosely coupled lattices in the difference formulation, since the linear stability analysis discussed in section 4 indicates that the  $2\Delta x$ -wave component receives no damping but very slight amplification for Scheme A. The growth of the  $2\Delta x$ -wave occurs eventually in experiments A, B, D, E, and I. Even though experiment A shows good total energy characteristics, a choppy pattern develops after about 65 days which makes the details of the solution very unrealistic. Figures 4a and 4b show the height field for experiment A after 50 and 100 days. At 50 days the choppy pattern is not noticeable but the 100-day map shows the development of a  $2\Delta x$ -wave pattern. In order to give some insight into the nature of the choppiness, the height map at 100 days is shown as two superimposed patterns; one shows the height field depicted by the grid points where  $j+k$  is an even number, and the other shows the height where  $j+k$  is an odd number, where  $j$  and  $k$  represent grid coordinates in the  $x$ - and  $y$ -direction respectively. Note that each is still very smooth but the two patterns are out of phase. The large differences between the two solutions indicate the

presence of large  $2\Delta x$  perturbation; the smoothness of each shows that the  $4\Delta x$ -wave component did not grow, as predicted from the stability analysis.

A display of the differences in the details of the solutions due to the differences in difference formulation and initial conditions is given in figure 5. Here the differences between the height field of experiment A and all the others are shown as the root mean square of the height differences defined by

$$\left[ \frac{1}{n} \sum_j \sum_k (h_{j,k}^X - h_{j,k}^A)^2 \right]^{1/2}$$

where  $j$  and  $k$  identify the grid position and  $n$  is the total number of grid points. Superscript  $A$  refers to experiment A and superscript  $X$  refers to any one of the others. Experiment A was chosen as the reference for this calculation since it shows the "best" total energy characteristics. Figure 5 shows that all the solutions differ significantly from experiment A by 50 days, a fact not clearly demonstrated in figure 3.

The value for the root mean square of the height differences is compared to the initial standard deviation in height on the right-hand scale in order to relate the magnitude of the differences between experiments to the magnitude of the variation in height originally present in each experiment. Note that according to the root mean square calculation, the subsequent differences due to small initial errors are of the same magnitude as those due to relatively small differences in the finite-difference equations. In other words, the sensitivity of the solution to the finite-difference formulation is similar to the sensitivity of the initial conditions for this particular example.

Figures 6a, 6b, and 6c show three height difference maps at 50 days to describe in more detail the differences between certain solutions. Figure 6a shows the difference due to a small amount of Fickian smoothing. Effects are largest in the regions of strongest velocity. Figure 6b shows differences due to boundary condition variations. Effects are largest near the northern boundary. Figure 6c shows differences due to small initial differences. Effects are again largest in the regions of largest fluid velocity. In the last diagram, the two lattice-separated solutions are shown individually, since by 50 days some separation of lattice effects had already appeared in the solution for experiment I. Note that the maximum difference in height in these three cases is at least twice as large as the root mean square of the height difference.

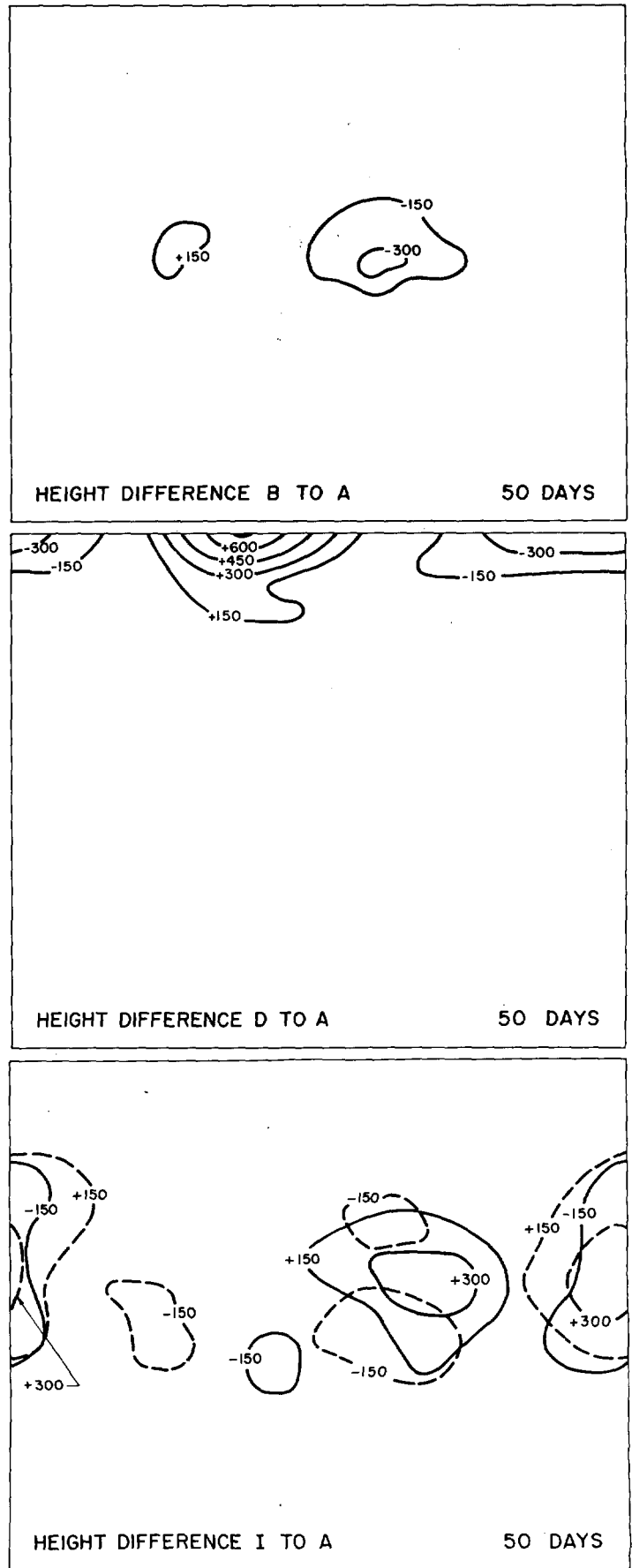


FIGURE 6.—Differences in height (m.) after 50 days between (a) experiments B and A; (b) experiments D and A; (c) experiments I and A. In (c) the solutions given by the two partial sets of the grid network are shown separately, with solid and dashed lines. See text.

## 7. REMARKS

The calculations show that it is possible to obtain a stable and relatively neutral long-term solution for a simple meteorological model without introducing a large amount of smoothing. Nevertheless, the schemes without a large degree of smoothing all developed unrealistic patterns in the solution possibly because of the separation of two different lattices. The calculations suggest that the two-step Lax-Wendroff scheme is useful for long-term integrations provided special care is given to the formulation of the Coriolis term and the control of truncation errors by smoothing.

The results show a sensitivity to changes in the finite-difference formulation which is significant after a long time period. The solutions also indicate that long-term truncation and stability effects are as important to the validity of long-term solutions as the growth of an initial error. This has bearing on the question of the practical upper limit to any long-term numerical integration from the standpoint of accuracy of the *details* in the solution. A study coordinated by Charney [1] has suggested an upper limit of several weeks because of inaccuracies in the initial conditions. It may well be that a similar practical upper limit exists because of truncation error and stability effects.

## ACKNOWLEDGMENTS

The authors wish to thank Eugene Isaacson who has read the original manuscript and offered useful comments. Joyce Takamine and Larry Williams assisted in programing the problems for the CDC 3600.

## REFERENCES

1. J. G. Charney, "The Feasibility of a Global Observation System," Report of Panel on International Meteorological Programs, Committee on Atmospheric Sciences, National Academy of Sciences, 1965, Section I, 48 pp.
2. P. D. Lax and B. Wendroff, "Systems of Conservation Laws," *Communications on Pure and Applied Mathematics*, vol. 13, 1960, pp. 217-237.
3. N. A. Phillips, "On the Problem of Initial Data for the Primitive Equations." *Tellus*, vol. 12, No. 2, May 1960, pp. 121-126.
4. L. F. Richardson, "Atmospheric Diffusion Shown on a Distance Neighbour Graph," *Proceedings of the Royal Society, Series A*, vol. 110, 1926, pp. 709-737.
5. R. D. Richtmyer, *Difference Methods for Initial-Value Problems*. Interscience Publishers, New York, 1957, 238 pp.
6. R. D. Richtmyer, "A Survey of Difference Methods for Non-Steady Fluid Dynamics," *NCAE Technical Notes 63-2*, National Center for Atmospheric Research, Boulder, Colo., 1963, 25 pp.
7. F. G. Shuman, "Numerical Experiments with the Primitive Equations," *Proceedings of the International Symposium on Numerical Weather Prediction in Tokyo*, Meteorological Society of Japan, Tokyo, 1962, pp. 85-107.
8. D. Williamson, "Stability of Difference Approximations to Certain Partial Differential Equations of Fluid Dynamics," National Center for Atmospheric Research, Boulder, Colo., Aug. 1965. (Manuscript submitted for publication.)

[Received September 28 1965; revised November 24, 1965]